

Impact of Complex Permeability Measurements Up to Millimeter-Wave Frequency Range

S. Yabukami^{1,2}, K. Nozawa², L. Tonthat², K. Okita¹, and R. Sai³

¹Graduate School of Biomedical Engineering, Tohoku University, Sendai 980-8579, Japan

²Graduate School of Engineering, Tohoku University, Sendai 980-8579, Japan

³Centre for Nano Science and Engineering, Indian Institute of Science, Bengaluru 560012, India

A highly sensitive microstrip-line-type probe using a flexible substrate was developed to measure thin-film permeability continuously up to the millimeter-wave frequency range (over 30 GHz). The probe enables broad bandwidth and highly sensitive permeability measurements without sample size limitations. The complex permeability of the CoFeB film (45 mm × 25 mm and 0.5 μm in thickness), CoNbZr film (25 mm × 25 mm and 3 nm in thickness), and nickel ferrite film (8 mm × 5 mm, and 1.2 μm in thickness) were optimized. The measured permeability spectrum and ferromagnetic resonance frequency showed good agreement with the theoretical values based on the Landau–Lifshitz–Gilbert equation and eddy current generation up to 67 GHz.

Index Terms—Complex permeability measurement, magnetic thin film, microstrip-line-type probe, millimeter-wave, sample size limitation.

I. INTRODUCTION

VARIOUS innovative thin-film applications such as magnetic sensors, spintronic devices, and high-frequency fifth-generation magnetic devices have dramatically increased the need to evaluate the high-frequency and highly sensitive permeability of magnetic thin films. Permeability measurement techniques are expected to increase in importance with bandwidths of millimeter-wave frequency range (over 30 GHz) and less than 10 nm film thickness. Nevertheless, almost all permeameters [1]–[3] require a special sample with a width up to several millimeters and a thickness of more than 100 nm. Few permeameters can measure thin films continuously with frequencies higher than 30 GHz. Therefore, many researchers and engineers of magnetic materials would welcome a broad bandwidth permeameter with no sample size limitations.

A microstrip-line-type probe using a bulky substrate has been developed in recent years [4]. However, the probe resonates at around 4.5 GHz because the microstrip line forms a right angle to the lead lines. Furthermore, because the probe substrate is made of bulky material and because the probe inflexibility prevents contact between the probe and the magnetic thin film, the probe is not always useful for evaluating very thin films, such as those of less than 10 nm in thickness. To overcome this shortcoming, we developed a straight microstrip-line-type probe on a flexible polyimide substrate [5]. The probe–film substrate contact surfaces fit very well, but the probe resonated at a frequency higher than 7 GHz because of impedance mismatch. It was not useful for large samples.

For this study, we built a new probe composed of a microstrip line on a flexible substrate with the microstrip

line sloping around 90° to meet the lead line at both ends. The probe flexibility enables contact between the microstrip conductor and a magnetic thin film, which enhances the signal-to-noise ratio. The probe, including the microstrip line and lead lines, has a characteristic impedance of around 50 Ω. The results show that the frequency range was significantly extended up to 67 GHz. A great benefit of this probe is that it can evaluate wafer-sized samples and can evaluate thin-film permeability irrespective of the sample size.

II. EXPERIMENTAL SETUP

A. New Probe and System Setup

Fig. 1(a) and (b) presents the views of the probe. Fig. 1(c) shows a photograph of the probe, which comprises a microstrip conductor (0.36 mm width) on a flexible substrate (RT/duroid at 5870, 123 μm in thickness, and $\epsilon_r = 2.3$), a ground plane, lead lines, and two connectors. The microstrip conductor is formed by etching one surface of the flexible substrate and placing a ground plane on the underside of the flexible substrate. The microstrip line has slopes to maintain a characteristic impedance of around 50 Ω and to allow close contact of a large sample with the probe. The flat tip of the microstrip line was about 1 mm. That part is set near the sample. By measuring the magnetic permeability of a smaller area, it can improve the spatial resolution. Furthermore, the slope bending angle was designed to be about 90° so as not to disturb the impedance matching. Coaxial cables are connected to a network analyzer. The probe can be bent easily because of the substrate flexibility, enabling a good fit between the probe and the thin film, thereby improving the signal-to-noise ratio. Fig. 2 portrays a photograph of the arrangement of the probe, a magnetic film, and an electromagnet. The system setup resembled those used in earlier studies [4]–[6]. A magnetic thin film was in contact with the microstrip conductor directly or via a 0.1 mm thick polyethylene terephthalate (PET) film.

Manuscript received May 8, 2020; revised June 30, 2020; accepted July 15, 2020. Date of publication July 27, 2020; date of current version January 20, 2021. Corresponding author: S. Yabukami (e-mail: yab@ecei.tohoku.ac.jp).

Color versions of one or more of the figures in this article are available online at <https://ieeexplore.ieee.org>.

Digital Object Identifier 10.1109/TMAG.2020.3011971

0018-9464 © 2020 IEEE. Personal use is permitted, but republication/redistribution requires IEEE permission.

See <https://www.ieee.org/publications/rights/index.html> for more information.

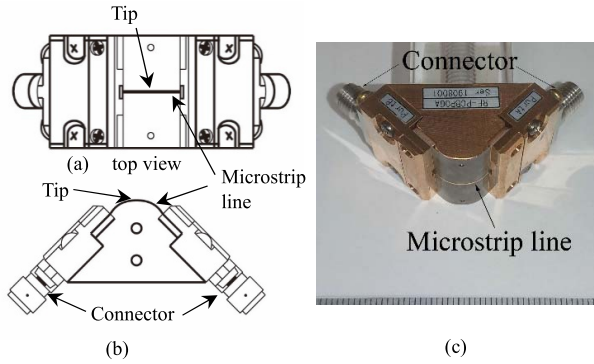


Fig. 1. Schematic and photographic view of the probe. (a) Top view. (b) Side view. (c) Photograph.

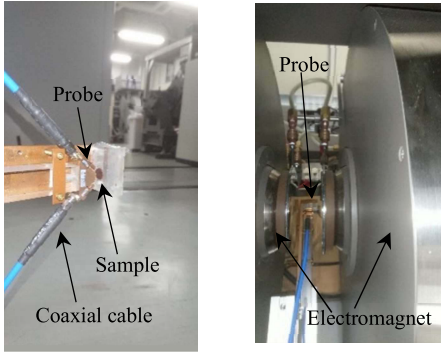


Fig. 2. Photograph of the probe and film.

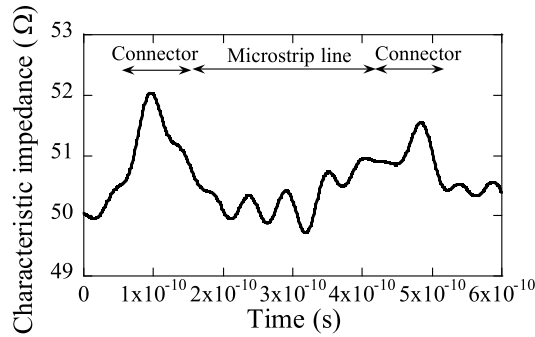


Fig. 3. Characteristic impedance of the probe obtained from TDR measurements.

Fig. 3 shows the distributed characteristic impedance of the probe measured using time-domain reflectometry (TDR) (N5227A; Agilent Technologies, Inc.). The characteristic impedance was 49.7–50.7 Ω along the microstrip line in proximity with the magnetic thin film and 49.7–52.0 Ω along the total probe including the connectors.

B. Optimization of Permeability

Fig. 4 presents a flowchart showing the permeability optimization. First, S_{21} is calibrated by application of a strong dc field (approximately 1590 kA/m; 20 kOe) in the direction of the easy axis to saturate the magnetic film. Second, S_{21} is measured without a strong dc field. The complex impedance is calculated using

$$Z_s = 100(1 - S_{21})/S_{21}. \quad (1)$$

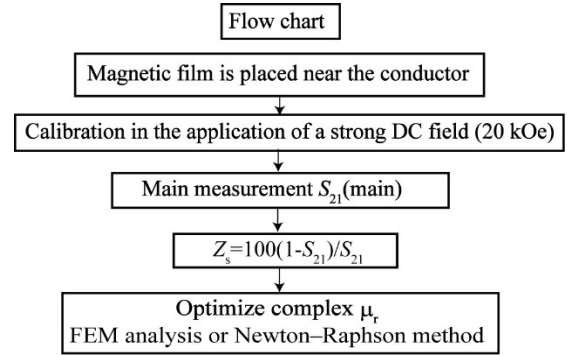


Fig. 4. Flowchart of the permeability measurements.

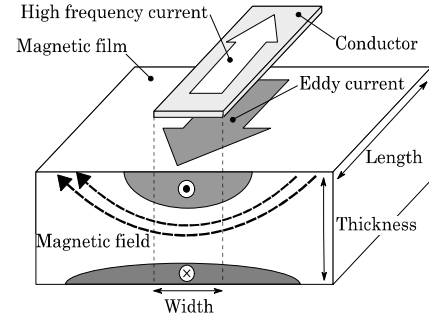


Fig. 5. Schematic of the eddy current and magnetic field in a film.

Equation (1) is derived from transmission line theory by placing the contribution of the magnetic thin film with a series impedance element Z_s [7]. The S_{21} and Z_s include multiple reflections in (1). The complex permeability of the uniaxial magnetic thin film is optimized using the Newton–Raphson method [8] to consider magnetic film skin effects with [6]

$$Z_s = \frac{kspl}{2w} \coth\left(\frac{k_s t}{2}\right) - \left\{ \frac{k'_s \rho l}{2w} \coth\left(\frac{k'_s t}{2}\right) \right\} \frac{1}{S_{21}} \quad (2)$$

$$k_s = \frac{(1+j)}{\sqrt{\frac{\rho}{\pi f \mu_r \mu_0}}} \quad k'_s = \frac{(1+j)}{\sqrt{\frac{\rho}{\pi f \mu_r^{ef} \mu_0}}} \quad (3)$$

In those equations, ρ stands for the resistivity of the film, t denotes the film thickness, l expresses the microstrip line length, w represents the microstrip conductor width, and μ_r^{ref} denotes the relative permeability when a strong dc field of 20 kOe (1590 kA/m) is applied. The high-frequency current induces a magnetic field in the width direction of the conductor pattern. The magnetic field and the eddy current are localized in the magnetic film skin, as presented in Fig. 5.

The complex permeability of magnetic material without anisotropy is optimized using finite element method (FEM) analysis. Fig. 6 shows the magnetic field calculation model and a cross-sectional view of the microstrip probe and magnetic thin film. Input high-frequency current was applied to the microstrip conductor and ground plane. The high-frequency magnetic field and eddy current distribution were calculated using the FEM analysis (Maxwell 2D; Ansoft Corporation). The calculated inductance was obtained from the integral of the magnetic field. The magnetic film permeability was changed from 1 to 1000 as a parameter. Fig. 7 presents the flux lines of the cross-sectional model of the microstrip line

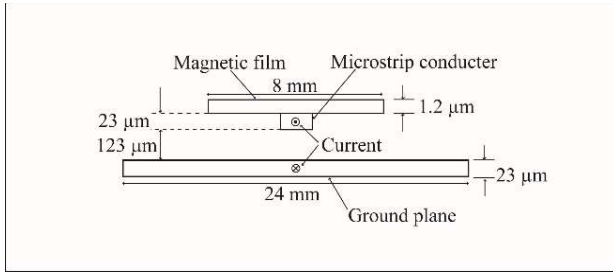


Fig. 6. Magnetic field calculation model by the FEM analysis.

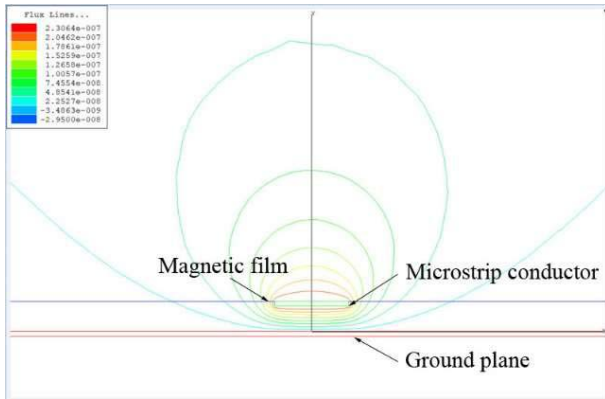


Fig. 7. Flux line of the cross-sectional model.

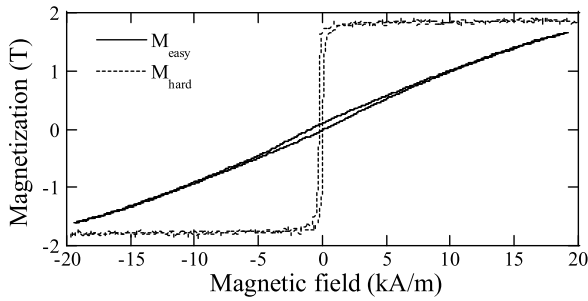


Fig. 8. MH curve of the CoFeB film.

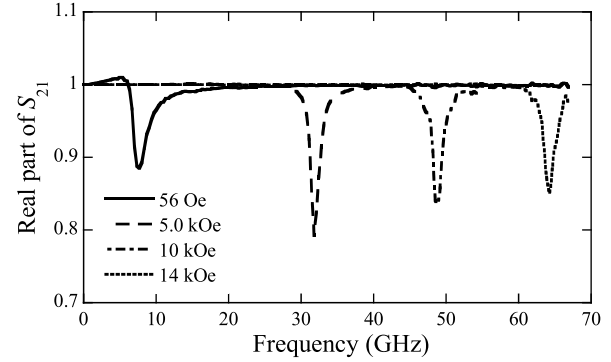
and magnetic thin film for a relative permeability of 2 and a 1 GHz frequency.

III. EXPERIMENTAL RESULTS

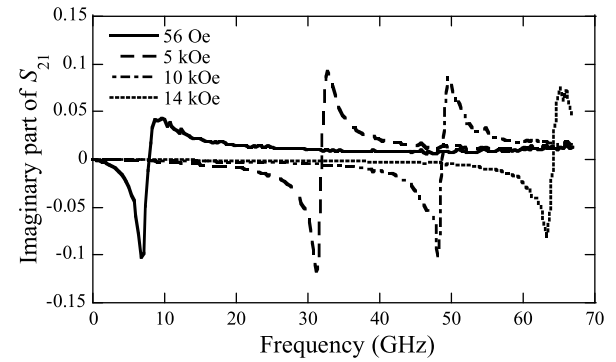
A. CoFeB Film

Fig. 8 shows the magnetization curve (MH curve) of the CoFeB film (45 mm \times 25 mm and 0.5 μ m in thickness) deposited by carousel sputtering [9]. Saturation magnetization around 1.8 T and an anisotropy field (H_k) of approximately 260 Oe (20.67 kA/m) was observed from the MH curve.

Fig. 9 shows the transmission coefficient (S_{21}) spectrum when the easy axis of the CoFeB film was parallel to the microstrip conductor [6]. Fig. 9(a) shows the real part of S_{21} . Fig. 9(b) shows the imaginary part of S_{21} when the bias fields of 56 Oe (4.452 kA/m), 5 kOe (397.5 kA/m), 10 kOe (795 kA/m), and 14 kOe (1113 kA/m) were applied along the easy axis. The S_{21} was first calibrated when the strong dc field of 20 kOe (1590 kA/m) was applied along the easy axis of the CoFeB film. The frequency range of the network analyzer (N5227A; Agilent Technologies, Inc.) was 10 MHz–67 GHz, the bandwidth was 1 kHz, the averaging number was 3, and



(a)

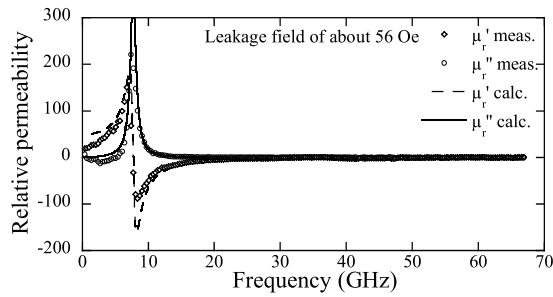


(b)

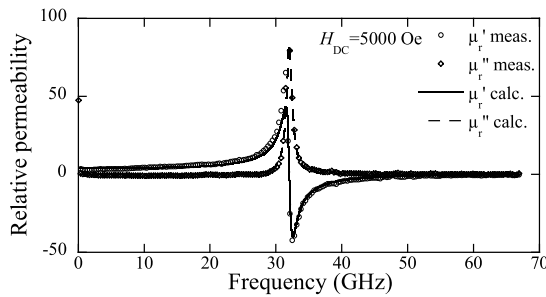
Fig. 9. S_{21} spectrum of the CoFeB film (25 mm \times 45 mm and 0.5 μ m in thickness). (a) Real part. (b) Imaginary part.

the RF power was 0 dBm. The real part of S_{21} corresponded to the imaginary part of permeability (μ''). Therefore, the dip frequencies were equal to the ferromagnetic resonance (FMR). However, the imaginary part of S_{21} corresponds to the real part of permeability (μ').

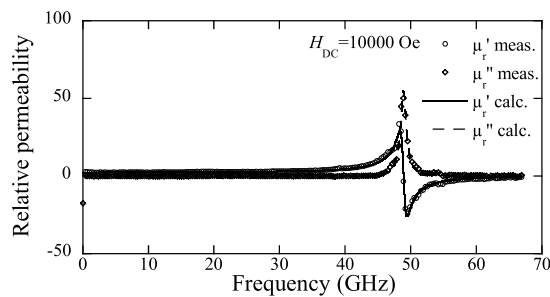
Fig. 10 shows the hard-axis permeability spectrum of the CoFeB film, which was optimized by the straight microstrip probe [6] and the Newton–Raphson method [8]. Fig. 10(a) shows the permeability without a dc current. Fig. 10(b)–(d) shows the permeability with the bias fields of 5 kOe (397.5 kA/m), 10 kOe (795 kA/m), and 14 kOe (1113 kA/m) applied along the easy axis. A small leakage field of about 56 Oe (4.452 kA/m) from the yoke existed even if the dc current was zero. The symbols show the measured permeability. The dotted lines and solid lines show the theoretical permeability based on the Landau–Lifshitz–Gilbert (LLG) equation and eddy current generation, respectively [10]. An α (damping factor) of 0.02, a g factor of 2.13 [11], and a resistivity of 140 $\mu\Omega\cdot\text{cm}$ were used to calculate the theoretical permeability. The absolute permeability was calibrated by application of dc magnetic fields in the easy-axis direction. The measured permeability was found to correspond to the theoretical permeability of up to 67 GHz. The FMR shifted from 8 to 67 GHz as the dc field increased. This limit of 67 GHz originated from the frequency band of the network analyzer (N5227A). Fig. 11 shows the FMR frequency as a function of the dc field. The symbols show the measured value. The solid line shows the theoretical value on the LLG equation and eddy current generation [10]. The results show



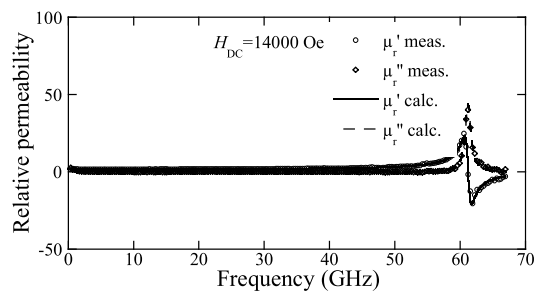
(a)



(b)



(c)



(d)

Fig. 10. Relative permeability of the CoFeB film (45 mm \times 25 mm and 0.5 μ m in thickness). (a) No dc field. (b) $H_{dc} = 5$ kOe (397.5 kA/m). (c) $H_{dc} = 10$ kOe (795 kA/m). (d) $H_{dc} = 14$ 000 Oe.

that the measured permeability and FMR frequency agreed well with the theoretical value up to 67 GHz.

B. Nickel Ferrite Film

Fig. 12 presents the complex permeability of the nickel ferrite film. The film was deposited using a low-temperature microwave-assisted solvothermal technique [12]. Fig. 13 shows a cross-sectional SEM image of the film. The S_{21} was measured using the probe in Fig. 1. Permeability was optimized by the relation between the permeability and the

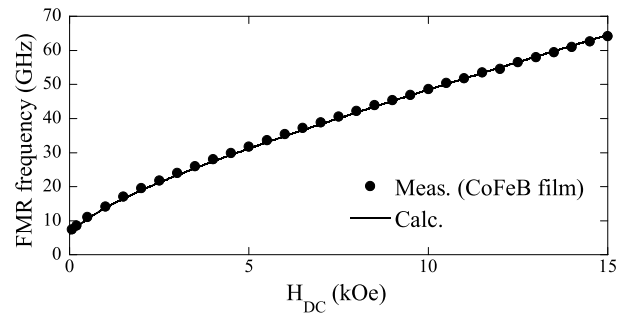


Fig. 11. FMR frequency as a function of applied dc field (45 mm \times 25 mm and 0.5 μ m in thickness).

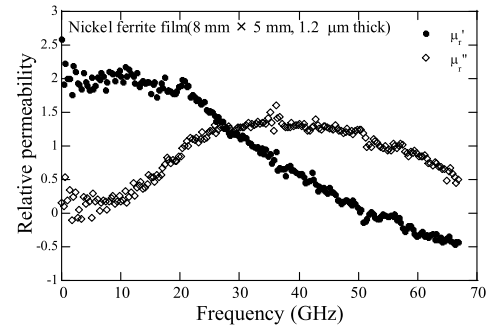


Fig. 12. Complex permeability of the nickel ferrite film (8 mm \times 5 mm and 1.2 μ m in thickness).

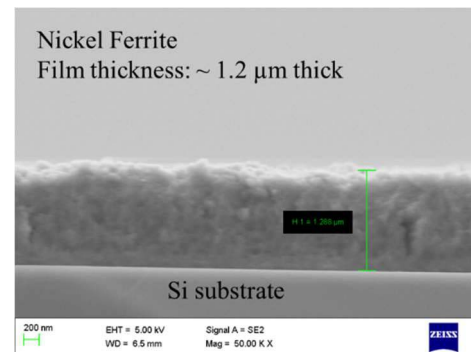


Fig. 13. SEM image of the nickel ferrite film [12].

inductance via the FEM analysis in Figs. 6 and 7. The real part of the permeability became negative at around 50 GHz. The imaginary part of the permeability showed a peak around 30–40 GHz. Very broadband FMR of the film was observed continuously using this permeameter.

C. CoNbZr Film

Fig. 14 shows the MH curves of a CoNbZr film (25 mm \times 25 mm and 3 nm in thickness) that was deposited by RF sputtering. The dotted line shows the MH curve of the easy axis. The solid line shows that of the hard axis. Very weak anisotropy was observed. The coercivity field was larger than the ordinary CoNbZr film, probably because the film was partly crystallized. Fig. 15 shows the hard-axis permeability of the CoNbZr film (25 mm \times 25 mm and 3 nm in thickness) when it was in contact with the flexible probe [6]. The symbols show the measured permeability. The dotted lines and the solid lines, respectively, show the theoretical permeability based on the LLG equation and

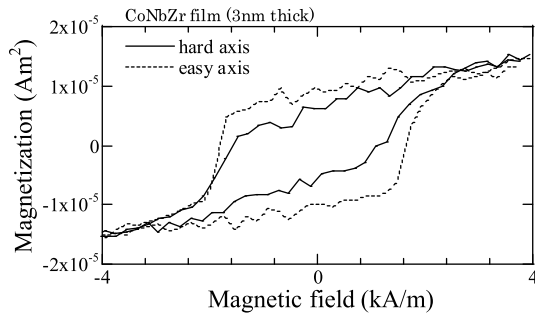


Fig. 14. MH curve of the CoNbZr film (25 mm × 25 mm and 3 nm in thickness).

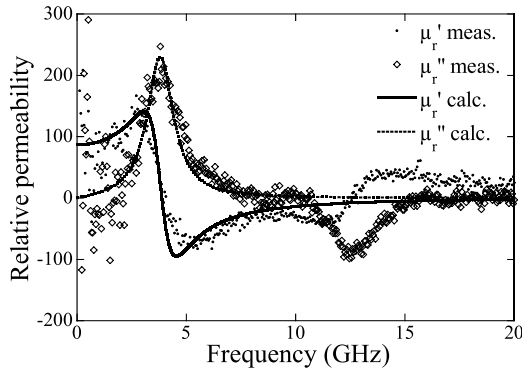


Fig. 15. Complex permeability of the CoNbZr film (25 mm × 25 mm and 3 nm in thickness).

eddy current generation [10]. A g factor of 2.13 [11] was used to calculate the theoretical permeability. An α (damping factor) of 0.04 was used to fit the theoretical permeability to the measured spectra. The measured permeability roughly corresponded to the theoretical permeability up to 12 GHz. The dc magnetic field of about 1.5 kOe (119.25 kA/m) in the background is insufficient to saturate the film because we used an aircore coil to remove the stray field of the yoke. Therefore, the FMR was observed at around 13 GHz. Because S_{21} is measured using this as a reference, when optimized for permeability, the FMR in the background around 13 GHz was observed as folded back; μ_r'' became negative. This phenomenon can be suppressed by increasing the value of the dc field.

IV. CONCLUSION

A very broadband probe was developed using a microstrip line and a flexible substrate for continuous measurement of thin-film permeability. The flexible probe enables good fit

between the probe and the thin film to enhance the signal-to-noise ratio. The probe is free from sample size limitations. A CoFeB film (45 mm × 25 mm and 0.5 μm in thickness), a CoNbZr film (25 mm × 25 mm and 3 nm in thickness), and a nickel ferrite film (8 mm × 5 mm and 1.2 μm in thickness) were evaluated. Their measured permeability and FMR frequencies showed good agreement with the theoretical values up to 67 GHz.

ACKNOWLEDGMENT

The authors thank Prof. Munakata, Sojo University, for providing the CoFeB film and Mr. Moriizumi, Candox Systems, for fabricating the probe. This work was supported in part by the Business Incubation Program (BIP) of Tohoku University and in part by the Ministry of Internal Affairs and Communications through Research and Development to Expand Radio Frequency Resources under Grant JPJ000254.

REFERENCES

- [1] P. A. Calcagno and D. A. Thompson, "Semiautomatic permeance tester for thick magnetic films," *Rev. Sci. Instrum.*, vol. 46, no. 7, pp. 904–908, 1975.
- [2] M. Yamaguchi, S. Yabukami, and K. I. Arai, "A new permeance meter based on both lumped elements/transmission line theories," *IEEE Trans. Magn.*, vol. 32, no. 5, pp. 4941–4943, Sep. 1996.
- [3] H. B. Weir, "Automatic measurement of complex dielectric constant and permeability at microwave frequencies," *Proc IEEE*, vol. 62, no. 1, pp. 33–36, Jan. 1974.
- [4] T. Kimura, S. Yabukami, T. Ozawa, Y. Miyazawa, H. Kenju, and Y. Shimada, "Permeability measurements of magnetic thin film with microstrip probe," *J. Magn. Soc. Jpn.*, vol. 38, nos. 1–3, pp. 87–91, 2014.
- [5] K. Kusunoki *et al.*, "Permeability measurements of very thin magnetic film using a flexible microstrip-line-type probe," *J. Magn. Soc. Jpn.*, vol. 39, no. 3, pp. 111–115, 2015.
- [6] S. Yabukami *et al.*, "Permeability measurements of thin film using a flexible microstrip line-type probe up to 40 GHz," *J. Magn. Soc. Jpn.*, vol. 41, no. 2, pp. 25–28, 2017.
- [7] A. A. Smith, *Radio Frequency Principles and Applications*, vol. 157. New York, NY, USA: IEEE Press, 1998.
- [8] W. H. Press, S. A. Teukolsky, W. T. Vetterling, and B. P. Flannery, *Numerical Recipes in C*, vol. 251, Japanese ed. Tokyo, Japan: Gijutsu Hyoron sha, 1993.
- [9] M. Namikawa *et al.*, "GHz permeability of soft magnetic Co-Fe-B films with high anisotropy fields," *J. Magn. Soc. Jpn.*, vol. 27, no. 4, pp. 371–374, 2003.
- [10] Y. Shimada, J. Numazawa, Y. Yoneda, and A. Hosono, "Absolute value measurements of thin film permeability," *J. Magn. Soc. Jpn.*, vol. 15, no. 2, pp. 327–330, 1991.
- [11] A. Yoshihara, K. Takanashi, M. Shimada, O. Kitakami, and Y. Shimada, "Magnon Brillouin scattering from an amorphous CoNbZr thin film," *Jpn. J. Appl. Phys.*, vol. 33, no. 7, p. 3927, 1994.
- [12] R. R. Kahmei, R. Sai, S. Arackal, S. Shivashankar, and N. Bhat, "Nanostructured Zn-substituted nickel ferrite thin films: CMOS-compatible deposition and excellent soft magnetic properties," *IEEE Magn. Lett.*, vol. 10, 2019, Art. no. 7106005.